

CrystEngComm

Accepted Manuscript



This is an *Accepted Manuscript*, which has been through the Royal Society of Chemistry peer review process and has been accepted for publication.

Accepted Manuscripts are published online shortly after acceptance, before technical editing, formatting and proof reading. Using this free service, authors can make their results available to the community, in citable form, before we publish the edited article. We will replace this *Accepted Manuscript* with the edited and formatted *Advance Article* as soon as it is available.

You can find more information about *Accepted Manuscripts* in the [Information for Authors](#).

Please note that technical editing may introduce minor changes to the text and/or graphics, which may alter content. The journal's standard [Terms & Conditions](#) and the [Ethical guidelines](#) still apply. In no event shall the Royal Society of Chemistry be held responsible for any errors or omissions in this *Accepted Manuscript* or any consequences arising from the use of any information it contains.

**Metal-controlled structural variations of coordination
architectures constructed from the flexible
1*H*-benzimidazole-1-propionic acid**

Zhong Zhang^{*}, Yan-Fang Feng, Qiu-Yu Wei, Kun Hu, Zi-Lu Chen and Fu-Pei Liang^{*}

Corresponding authors

Zhong Zhang and Fu-Pei Liang

Affiliation and address

Key Laboratory for the Chemistry and Molecular Engineering of Medicinal Resources (Ministry of Education of China), School of Chemistry and Pharmacy of Guangxi Normal University, Guilin 541004, P. R. China

E-mail address, telephone and fax numbers of the corresponding authors

e-mail: zhangzhong@mailbox.gxnu.edu.cn

telephone: +86-773-5854878

fax: +86-773-5832294

† Electronic supplementary information (ESI) available: Simulated and calculated PXRD patterns (Fig. S1), TG curves (Fig. S2), luminescence excitation spectra (Fig. S3), selected bond distances (Table S1) and selected hydrogen bond parameters (Table S2) for complexes **1–6**. CCDC reference numbers 1406660–1406665 for **1–6**. For ESI and crystallographic data in CIF or other electronic format see

Abstract

Treatment of a flexible bifunctional ligand 1*H*-benzimidazole-1-propionic acid (Hbiap) with appropriate transition metal salts led to the formation of six new complexes, [Co(biap)₂]_n (**1**), [Cu₂(biap)₄(H₂O)]_n · 7n(H₂O) (**2**), [Ag(H_{0.5}biap)₂]_n · 2n(H₂O) (**3**), [Zn(biap)₂]_n (**4**), [Cd₁₂(biap)₂₄] · 8H₂O (**5**) and [Hg(Hbiap)Cl₂] (**6**). X-ray crystallographic studies reveal that complexes **1** and **2** exhibit two different 1D chain structures due to the distinct coordination geometries of central Co(II) and Cu(II). Complex **3** consists of a 1D zigzag [Ag(H_{0.5}biap)₂]_n chain constructed *via* O··H··O interactions. Within **4**, two sets of 1D [Zn(biap)]_n chains along two perpendicular directions are interwoven at Zn(II) nodes to afford a 2D puckered sheet with (4,4) topology. The crystal structure of **5** manifests an unprecedented nano-sized dodecanuclear Cd(II) cage in a garland-like appearance, which can be thought of as a head-to-tail 1D looped chain enclosing a hollow cavity. Complex **6** features a 1D infinite wavy chain generated by the linkage of [Hg(Hbiap)₂] and HgCl₂ fragments through μ₂-Cl groups. In these complexes, the flexible organic ligand is in favor of the *gauche* conformation in **1–5**, and the *anti* conformer only can be observed in **6**. A comparison of the structural features for these complexes suggests that the coordination preferences of metals, connectivity of metal nodes as well as binding modes and protonation behavior of Hbiap are responsible for the interesting architectural variations. Four coordination complexes with *d*¹⁰ metal centers display solid-state luminescent emissions under room temperature, which originate from either intraligand π–π* transitions (**4** and **5**) or ligand to metal charge transfer (LMCT) transitions (**3** and **6**).

Introduction

The design and construction of metal-organic materials, such as discrete metal-organic clusters and extended metal-organic polymers, has been still a hot research topic in coordination chemistry and materials science because of their fascinating structures and unique functions.¹ A number of previous investigations in this respect have proven that the subtle selection of the organic ligands with appropriate functional groups, suitable arrangement of the donor groups, specific geometric configuration and conformational flexibility is the key step in the pre-designed assembly of the novel metal-organic architectures.² Owing to the abundant available metal binding sites, high

binding affinity and tunable coordination patterns, rigid bifunctional ligands composed of both azole moieties and carboxylic groups have been preferred as the organic linkers utilized in the directional preparation of the metal-organic polymers exhibiting intriguing topological structures³ and potential applications as fluorescent devices,⁴ magnetic materials,⁵ and in gas adsorption,⁶ gas separation,⁷ catalysis⁸ and proton conduction.⁹ In contrast to the rigid ligands, the flexible analogues of the rigid species employed in the assembly of the coordination structures have seemed more challenging but attracted more and more attentions as the flexibility of the ligands can facilitate the formation of diversified structural motifs and unusual properties.¹⁰ In recent years, many intricate metal-organic coordination complexes with diverse structures from 0D to 3D and interesting physicochemical properties have been fabricated from several flexible azole derivatives bearing acetic acid group.¹¹ It is worth to be mentioned that the binding modes and even the geometric conformations of these flexible ligands are sensitive to many factors such as metal ions,¹² pH value,¹³ counter anions¹⁴ and synthetic methods,¹⁵ which make a rational prediction on the structures and functions of their coordination complexes unfeasible in a majority of the cases. Therefore, more systematic studies must be undergone in correlation the assembled structures with the coordination and conformation versatility of the flexible azole-containing ligands. These further efforts undoubtedly may provide deeper insights into the pre-designed and controllable fabrication of the target coordination complexes.

Motivated by the previous studies, we had made use of two azole compounds bearing propionic acid functional group as more flexible organic connectors to build up extended coordination polymers and revealed that the resulting assembled structures can be tuned by choosing azole carboxylic acid ligands bearing different length spacers.¹⁶ To extend our research on the coordination chemistry of this series of azole-containing ligands and explore the directing capability of different metal ions on the architectural motifs of their complexes. Herein, a flexible bifunctional ligand, namely *1H*-benzimidazole-1-propionic acid (Hbiap), has been mixed with Co(II), Cu(II), Ag(I), Zn(II) and Cd(II) nitrates as well as HgCl₂ individually under two distinct synthetic pathways, affording six new metal-organic coordination complexes **1–6** varying from discrete high-nuclearity coordination cage to 2D polymeric network. A detailed structural comparison of these complexes has been carried out so as to clarify the effect of the conformational freedom and

coordination modes of Hbiap (Scheme 1) along with the coordination natures and connectivity of different metal ions on the structural variations. In addition, the solid-state luminescence properties of Hbiap and its d^{10} transition metal complexes 3–6 have been presented and discussed.

Scheme 1 is here

Scheme 1. Three coordination modes of ligand Hbiap observed in complexes 1–6.

Experimental section

Materials and methods

All reagents used for the syntheses of ligands and metal complexes were commercially available and applied without further purification. The heterocyclic ligand 1*H*-benzimidazole-1-propionic acid was synthesized according to a published document.¹⁷

C, H, N elemental analyses were performed on an Elementar Vario Micro Cube elemental analyzer. IR spectra were recorded on a Perkin–Elmer Spectrum One FTIR spectrometer as KBr pellets in the 400–4000 cm^{-1} region. Thermogravimetric analysis was obtained using a Setaram Labsys Evo TG–DTA/DSC instrument at a heating rate of 10 $^{\circ}\text{C}/\text{min}$ under a nitrogen atmosphere in the temperature range of 30–800 $^{\circ}\text{C}$. The luminescence spectra were performed on a Horiba Jobin–Yvon FL3-P-TCSPC fluorescence spectrometer in the solid state at room temperature. Powder X-ray diffraction measurements (PXRD) for poly-crystalline samples of all complexes were performed on a Rigaku D/Max-2500 V diffractometer equipped with Cu– $K\alpha$ radiation ($\lambda = 1.54178 \text{ \AA}$) in the 2θ range from 5 $^{\circ}$ to 60 $^{\circ}$.

X-ray data collection and structure determination

Single-crystal X-ray diffraction measurements were performed on a Bruker Smart APEX II diffractometer using graphite-monochromated Mo- $K\alpha$ radiation (0.71073 \AA). Empirical absorption correction was applied to raw intensities with the SADABS program.¹⁸ The program SAINT was used for integration of the diffraction profiles.¹⁹ All structures were solved by direct methods using the SHELXS program of the SHELXTL software package and refined with SHELXL program.²⁰ All non-hydrogen atoms were located in successive difference Fourier syntheses and subjected to anisotropic refinement. The hydrogen atoms of carboxylic groups and water

molecules were located from difference Fourier maps and refined isotropically with $U_{\text{iso}}(\text{H}) = 1.5 U_{\text{eq}}(\text{O})$, all other hydrogen atoms were located in geometric positions and refined with a riding model. The experimental details for data collections and refinement of complexes **1–6** are summarized in Table 1. Selected bond distances for all complexes and selected hydrogen bond parameters for complexes **2**, **3** and **6** are presented in Table S1 and S2.

Synthesis of $[\text{Co}(\text{biap})_2]_n$ (**1**)

Treating the aqueous solution (2 mL) of $\text{Co}(\text{NO}_3)_2 \cdot 6\text{H}_2\text{O}$ (0.087 g, 0.30 mmol) with an equimolar amount of 1*H*-benzimidazole-1-propionic acid (Hbiap) (0.057 g) dissolved in water (4 mL). The mixture was stirred in the hot water bath at 80 °C for 4 h. After cooling, the solution was allowed to stand at room temperature. After evaporation of the solvent for one month, purple block crystals of **1** were obtained, which were washed with cooled water and dried in air (0.027 g, yield 61%). Anal. Calcd for $\text{C}_{40}\text{H}_{36}\text{Co}_2\text{N}_8\text{O}_8$: C, 54.93; H, 4.15; N, 12.81%. Found: C, 54.83; H, 4.09; N, 12.64 %. IR (KBr pellet, cm^{-1}): 3445(m), 3138(w), 3109(w), 2957(w), 1621(s), 1610(s), 1504(w), 1484(w), 1460(m), 1415(s), 1401(s), 1358(w), 1294(m), 1260(m), 1193(m), 1052(w), 983(w), 955(w), 912(w), 751(m), 739(m), 600(w), 557(w), 528(w).

Synthesis of $[\text{Cu}_2(\text{biap})_4(\text{H}_2\text{O})]_n \cdot 7n(\text{H}_2\text{O})$ (**2**)

A mixture of Hbiap (0.076 g, 0.30 mmol) and $\text{Cu}(\text{NO}_3)_2 \cdot 6\text{H}_2\text{O}$ (0.036 g, 0.15 mmol) in 8 ml distilled water was sealed in a 25 ml Teflon-lined stainless steel autoclave. The autoclave was heated at 120 °C for 48 h and then slowly cooled to ambient temperature over a 24 h period. Green block crystals of **2** were obtained and collected by filtration, washed with water and dried in air (0.037 g, yield 48%). Anal. Calcd for $\text{C}_{40}\text{H}_{52}\text{Cu}_2\text{N}_8\text{O}_{16}$: C, 46.74; H, 5.10; N, 10.90%. Found: C, 46.35; H, 4.86; N, 10.91%. IR (KBr pellet, cm^{-1}): IR (KBr pellet, cm^{-1}): 3445(s), 3157(w), 3109(w), 2990(w), 1622(s), 1566(m), 1485(w), 1432(m), 1384(s), 1319(m), 1284(m), 1243(w), 1190(w), 1039(w), 995(w), 943(w), 912(w), 879(w), 760(m), 643(m), 614(w), 517(w).

Table 1 Crystallographic data and structure refinement summary for complexes 1–6

Complexes	1	2	3	4	5	6
Empirical formula	C ₄₀ H ₃₆ Co ₂ N ₈ O ₈	C ₄₀ H ₅₂ Cu ₂ N ₈ O ₁₆	C ₂₀ H ₂₃ AgN ₄ O ₆	C ₂₀ H ₁₈ N ₄ O ₄ Zn	C ₂₄₀ H ₂₃₂ Cd ₁₂ N ₄₈ O ₅₆	C ₁₀ H ₁₀ Cl ₂ HgN ₂ O ₂
Formula weight	874.63	1027.98	523.29	443.75	6033.54	461.69
Temperature/K	294(2)	294(2)	294(2)	294(2)	294(2)	294(2)
Wavelength/Å	0.71073	0.71073	0.71073	0.71073	0.71073	0.71073
Crystal system	Triclinic	Monoclinic	Monoclinic	Monoclinic	Trigonal	Monoclinic
Space group	<i>P</i> $\bar{1}$	<i>P</i> 2(1)/ <i>c</i>	<i>C</i> 2/ <i>c</i>	<i>P</i> 2(1)/ <i>c</i>	<i>R</i> $\bar{3}$	<i>P</i> 2(1)/ <i>c</i>
<i>a</i> /Å	9.2206(18)	26.010(11)	24.081(8)	13.2788(2)	27.288(4)	14.897(8)
<i>b</i> /Å	14.881(3)	10.830(5)	6.4039(8)	8.36930(10)	27.288(4)	10.377(6)
<i>c</i> /Å	15.697(3)	15.972(7)	16.283(4)	16.8959(4)	32.044(6)	8.216(5)
α /°	115.13(3)	90	90	90	90	90
β /°	92.57(3)	90.758(7)	121.64(4)	102.025(2)	90	90.647(8)
γ /°	99.02(3)	90	90	90	120	90
Volume/Å ³	1910.7(7)	4498(3)	2137.9(9)	1836.51(6)	20664(6)	1270.0(13)
<i>Z</i>	2	4	4	4	3	4
Calculated density/g cm ⁻³	1.520	1.518	1.626	1.605	1.455	2.415
Absorption coefficient/mm ⁻¹	0.934	1.025	0.987	1.374	0.985	12.530
<i>F</i> (000)	900	2136	1064	912	9096	856
θ range for data collection	2.83 to 26.00	0.78 to 26.00	2.94 to 24.97	3.02 to 26.50	2.99 to 26.00	1.37 to 26.00
Crystal size/mm ³	0.31×0.28×0.25	0.20×0.17×0.13	0.24×0.11×0.09	0.33×0.24×0.22	0.30×0.24×0.18	0.26×0.22×0.20
Reflections collected	7488	8830	1887	3803	9033	2496
Independent reflections	5060	6798	1195	3218	6695	2232
Data/restraints/parameters	7488/523/0	8830/595/1	1887/145/1	3803/263/0	9033/550/0	2496/156/0
Goodness-of-fit on <i>F</i> ²	1.006	1.037	1.093	1.003	1.091	1.043
<i>R</i> ₁ ^a / <i>wR</i> ₂ ^b (<i>I</i> >2σ(<i>I</i>))	0.0520/0.1017	0.0396/0.1037	0.0655/0.1829	0.0349/0.0844	0.0421/0.1055	0.0221/0.0654
<i>R</i> ₁ ^a / <i>wR</i> ₂ ^b (all data)	0.0856/0.1159	0.0580/0.1122	0.0976/0.2105	0.0426/0.0887	0.0509/0.1069	0.0268/0.0676
Largest difference peak and hole /e Å ⁻³	0.380 and -0.360	0.440 and -0.425	1.054 and -0.375	0.420 and -0.526	0.686 and -0.409	0.930 and -1.349

^a $R_1 = \sum ||F_o| - |F_c|| / \sum |F_o|$. ^b $wR_2 = \{ \sum [w(F_o^2 - F_c^2)]^2 / \sum [w(F_o^2)]^2 \}^{1/2}$.

Synthesis of $[\text{Ag}(\text{H}_{0.5}\text{biap})_2]_n \cdot 2n(\text{H}_2\text{O})$ (**3**)

Complex **3** was prepared according to the procedure described for **2** except that AgNO_3 (0.028 g, 0.15 mmol) was used instead of $\text{Cu}(\text{NO}_3)_2 \cdot 6\text{H}_2\text{O}$ to react with two equivalent amount of Hbiap. Colorless needle crystals were obtained and collected by filtration, washed with water and dried in air (0.051 g, yield 65%). Anal. Calcd for $\text{C}_{20}\text{H}_{23}\text{AgN}_4\text{O}_6$: C, 45.90; H, 4.43; N, 10.71%. Found: C, 45.63; H, 4.61; N, 10.37 %. IR (KBr pellet, cm^{-1}): 3390(m), 3109(w), 3046(w), 2942(w), 1701(m), 1654(m), 1578(s), 1507(s), 1461(m), 1445(m), 1383(m), 1292(m), 1258(m), 1120(m), 1044(w), 1006(w), 947(w), 906(w), 939(w), 868(w), 839(w), 776(w), 739(s), 634(w), 428(w).

Synthesis of $[\text{Zn}(\text{biap})_2]_n$ (**4**)

Complex **4** was prepared in a similar way as for **1** except that $\text{Zn}(\text{NO}_3)_2 \cdot 6\text{H}_2\text{O}$ (0.045 g, 0.15 mmol) was used instead of $\text{Co}(\text{NO}_3)_2 \cdot 6\text{H}_2\text{O}$ to react with two equivalent amount of Hbiap. Colorless block crystals were collected within half a month (0.025 g, yield 37%). Anal. Calcd for $\text{C}_{20}\text{H}_{18}\text{ZnN}_4\text{O}_4$: C, 54.13; H, 4.09; N, 12.63%. Found: C, 53.95; H, 4.32; N, 12.52 %. IR (KBr pellet, cm^{-1}): 3434(m), 3119(w), 2956(w), 2922(w), 1633(s), 1615(s), 1512(m), 1483(w), 1467(m), 1449(m), 1410(s), 1397(s), 1384(s), 1360(m), 1335(w), 1288(s), 1262(m), 1234(w), 1196(w), 1184(w), 953(w), 932(w), 916(w), 864(w), 777(w), 763(w), 739(m), 634(w), 575(w), 525(w).

Synthesis of $[\text{Cd}_{12}(\text{biap})_{24}] \cdot 8\text{H}_2\text{O}$ (**5**)

Complex **5** was prepared in a similar way as for **1** except that $\text{Cd}(\text{NO}_3)_2 \cdot 4\text{H}_2\text{O}$ (0.090 g, 0.30 mmol) was used instead of $\text{Co}(\text{NO}_3)_2 \cdot 6\text{H}_2\text{O}$ to react with equivalent amount of Hbiap. Colorless block crystals were obtained after one month (0.019 g, yield 25%). Anal. Calcd for $\text{C}_{240}\text{H}_{232}\text{Cd}_{12}\text{N}_{48}\text{O}_{56}$: C, 47.78; H, 3.88; N, 11.14%. Found: C, 47.67; H, 3.66; N, 11.31%. IR (KBr pellet, cm^{-1}): 3438(s), 3112(w), 2932(w), 1633(s), 1506(m), 1426(m), 1386(m), 1311(w), 1296(w), 1262(m), 1190(m), 1115(m), 1052(w), 946(w), 908(w), 878(w), 745(m), 632(m), 602(m).

Synthesis of $[\text{Hg}(\text{Hbiap})\text{Cl}_2]$ (**6**)

Complex **6** was prepared in a similar way as for **1** except that HgCl_2 (0.027 g, 0.10 mmol) was used instead of $\text{Co}(\text{NO}_3)_2 \cdot 6\text{H}_2\text{O}$ to react with equivalent amount of Hbiap. Colorless block crystals were obtained after two weeks (0.041 g, yield 82%). Anal. Calcd for $\text{C}_{10}\text{H}_{10}\text{Cl}_2\text{HgN}_2\text{O}_2$: C, 49.40; H, 1.88; N, 5.24%. Found: C, 49.34; H, 1.65; N, 5.44%. IR (KBr pellet, cm^{-1}): 3443(s), 3120(w), 2964(w), 2930(w), 1699(m), 1625(s), 1595(s), 1511(w), 1437(w), 1417(m), 1386(m), 1315(w), 1262(m), 1193(w), 1097(m), 1028(m), 933(w), 874(w), 804(m), 747(m), 623(w), 497(m), 421(w).

Result and discussion

Syntheses and general characterization

The neutral metal complexes reported here were prepared by conventional aqueous solution reaction or hydrothermal procedure between the flexible ligand and appropriate metal salts in different stoichiometric ratios of 1:1 or 2:1. All isolated complexes were characterized by elemental analysis, infrared spectra, X-ray single crystal determination and powder X-ray diffraction (PXRD). The IR spectra of complexes **3** and **6** reveal the vibration absorbance of carboxyl group at 1701 cm^{-1} or 1699 cm^{-1} , which is the signal of partial deprotonation and/or protonation of the original carboxylic acid ligand. Apart from them, the carboxylic acid functionality of Hbiap in the other solid complexes is completely deprotonated since some characteristic absorption peaks due to the ν_{as} and ν_{s} stretching of carboxylate group appear in the spectral ranges of $1610\text{--}1640\text{ cm}^{-1}$ and $1400\text{--}1440\text{ cm}^{-1}$, respectively. These results were further testified by the solid-state X-ray single crystal diffraction method. The bulky as-synthesized samples of complexes **1–6** were subject to PXRD analysis. As shown in Fig. S1, the experimental diffraction patterns of these complexes match well with the simulated ones obtained from the single-crystal diffraction data, confirming the phase purity of the as-synthesized products.

Crystal structure description

Complex **1** reveals a 1D looped chain structure and crystallizes in the triclinic crystal system with the space group of $P\bar{1}$. The asymmetric unit consists of two crystallographically independent Co(II) ions and four anionic biap⁻ ligands (Fig. 1a). Co1 or Co2 ion in **1** locates in a tetrahedral

coordination environment, defined by two benzimidazole N atoms and two carboxylate O atoms from four different ligands. The Co–O and Co–N bond lengths fall in the range of 1.932(2) and 2.045(3) Å, comparable to those found for the reported Co(II)-carboxylate or Co(II)-benzimidazole complexes.^{11c,21} The bidentate biap[−] ligand as a μ_2 -bridge (mode a) binds to two Co(II) ions through one imidazole N atom and one carboxylate O atom. All bridging ligands in this compound assume the *gauche* conformation with the N–C–C–C torsion angles around the ethylene spacer approaching to -66° or $+75^\circ$. Each Co ion is bonded to two adjacent Co ions through two pairs of bridging biap[−], to constitute an infinite 1D polymeric looped chain parallel to the *b* axis (Fig. 1b). There exist two inequivalent boat-like [Co₂(biap)₂] rings in this 1D polymeric chain with the intra-ring Co1⋯Co2 separations alternating between 7.427(2) and 7.563(2) Å. Arising from the geometric demand of the central ions, two benzimidazole fragments of either one of the bimetallic rings are twisted to each other by a dihedral angle of 84.96(7)° or 54.03(8)°, respectively. Weak $\pi\cdots\pi$ stacking interactions could be observed between the benzimidazole rings (centroid-to-centroid distance of 3.647 Å) of two adjacent 1D chains, thus a double looped chain aggregate is generated (Fig. 1c).

Fig. 1a is here

(a)

Fig. 1b is here

(b)

Fig. 1c is here

(c)

Fig. 1 (a) The coordination environments around Co(II) ions in **1** (symmetry codes: A $x, 1+y, z$; B $x, -1+y, z$). (b) View of the 1D looped chain extending along the *b* axis. Co, pink; C, grey; N, blue; O, red. (c) Two 1D looped chains are joined by interchain $\pi\cdots\pi$ stacking interactions into a double chain aggregate. Hydrogen atoms are omitted for clarity.

X-ray structural analysis shows that complex **2** is a 1D undulated double-chain polymer and crystallizes in the monoclinic crystal system with the space group of $P2_1/c$. There are two chemically inequivalent Cu(II) ions, four biap[−] ligands, one coordinated water molecule and seven

lattice water molecules in the asymmetric unit. As shown in Fig. 2a, Cu1 center adopts a penta-coordinated square-pyramidal geometry, whose equatorial plane consists of two N and two O donors from four organic connectors in *trans* arrangement and the apical position is occupied by a water O atom. Owing to Jahn–Teller effect, the apical Cu1–O9 bond distance (2.409(2) Å) is apparently longer than those of equatorial ones in the range from 1.975(2) to 2.011(2) Å.²² Unlike Cu1, Cu2 center is tetra-coordinated to two N atoms and two O atoms from four ligands, completing a square planar coordination sphere. The bond lengths of two Cu2–O are nearly equal, but slightly shorter than those of Cu2–N bonds. The biap[−] ligands all take μ_2 -bridging coordination mode (mode a), and the values of the torsion angles around the central C–C bond (N1–C8–C9–C10 = 63.46(31) °, N3–C18–C19–C20 = 68.07(29) °, N5–C28–C29–C30 = −64.42(30) ° and N7–C38–C39–C40 = −67.20(30) °) indicate the *gauche* conformation of four independent ligands. Two biap[−] combine two Cu(II) ions to form a [Cu₂(biap)₂] metalla-ring, which propagates along the (1 0 −2) direction to afford a 1D undulated double-chain wherein the Cu⋯Cu distances are 7.714(3) Å for Cu1⋯Cu1, 7.522(3) Å for Cu2⋯Cu2 and 7.768(3) Å for Cu1⋯Cu2 (Fig. 2b). Constrained by the geometric requirements of the Cu(II) ions, this chain reveals some structural differences from that in **1**. In each bimetallic ring, the benzimidazole groups of both ligands are almost parallel to each other, whilst the benzimidazole groups from the adjacent rings are arranged evenly on the opposite sides of the chain. A 3D hydrogen bonding network constructed from the 1D polymeric chain is stabilized by the multiple O–H⋯O hydrogen bonding interactions occurring between carboxylate O atoms of the ligand, coordinated water and lattice water molecules (Fig. 2c).

Fig. 2a is here

(a)

Fig. 2b is here

(b)

Fig. 2c is here

(c)

Fig. 2 (a) The coordination environments around Cu(II) ions in **2** (symmetry codes: A $-x, y, 3/2-z$; B $1-x, y, 1/2-z$). (b) The 1D undulated double-chain of **2**. Cu, aqua; C, grey; N, blue; O, red. (c) The 3D supramolecular framework formed by O–H⋯O hydrogen bonds. Hydrogen atoms not

involved in hydrogen bonding are omitted for clarity.

Complex **3** is composed of a 1D zigzag chain formed by O··H··O interactions, whose structure is similar to the Ag(I) compound containing 1*H*-benzimidazole-1-acetic acid.^{11a} Hbiap only functions as a monodentate ligand in this complex with one benzimidazole N donor bound to the central Ag(I) (mode b). The uncoordinated carboxylic acid group of the ligand is half dissociated, and in the difference Fourier map one proton can be located on the middle point of two head-to-head arranged carboxylic groups from two H_{0.5}biap ligands. The central Ag(I) is bound to two N atoms belonging to two different H_{0.5}biap ligands resulting in a [Ag(H_{0.5}biap)₂] unit (Fig. 3a). As the metal center is disordered over two positions around the inversion center with site-occupancy factor of 0.5, two Ag–N bond distances of 1.969(6) and 2.359(8) Å in such a coordination unit are not equivalent. The O··O separation of 2.462(8) Å is indicative of a O··H··O interaction between neighboring carboxylic groups clearly, with which [Ag(H_{0.5}biap)₂] entities are linked into a 1D infinite single chain (Fig. 3b). Within the chain, the ligand possesses a *gauche* conformation with the torsion angle across the central C–C bond of +69.36(98)°, and the benzimidazole groups of all ligands are parallel to each other. Additionally, inter-chain π··π stacking between imidazole and phenyl rings with centroid-to-centroid distance of 3.863 Å extend 1D infinite chains into a 2D supramolecular matrix (Fig. 3c).

Fig. 3a is here

(a)

Fig. 3b is here

(b)

Fig. 3c is here

(c)

Fig. 3 (a) The coordination environment around Ag(I) ion in **3** (symmetry code: A $1/2-x, 1/2-y, 1-z$). (b) The 1D zigzag chain formed by O··H··O interactions viewed along the *a* direction. Ag, aqua; C, grey; H, light grey; N, blue; O, red. (c) The 2D sheet sustained by interchain π··π stacking interactions. All solvent molecules and hydrogen atoms not involved in O··H··O interactions are omitted for clarity.

Complex **4** features a 2D polymeric layer with (4,4) topological network. The asymmetric unit contains one Zn(II) center and two distinct anionic biap⁻ ligands. The environment of central Zn(II) is tetrahedral, coordinated to two benzimidazole N atoms and two carboxylate O atoms provided by four ligands (Fig. 4a). The Zn–O bond distances vary from 1.954(2) to 1.955(2) Å, and Zn–N separations range from 2.033(2) to 2.035(2) Å, both are in agreement with those found for the analogues tetrahedral Zn(II) complexes.^{21,23} Although ligand biap⁻ also serves as a two-connected linker (mode a) and exists as a *gauche* conformer, the connectivity of the metal node in this complex differs from those found in **1** and **2**. One Zn(II) ion acts as a four-connected node to link other four Zn(II) ions *via* four biap⁻ linkers, as a comparison each Co(II) in **1** or Cu(II) in **2** only connects with two neighboring metal ions. The heterocyclic ligands with their benzimidazole moieties nearly perpendicular to the *bc* plane join Zn(II) ions into 1D wave-like [Zn(biap)]_n chains running along the *c* axis, meanwhile the remaining ligands with their benzimidazole moieties inclined to the same plane extend Zn(II) ions to another set of 1D [Zn(biap)]_n chains lying along the *b* axis. It is noticed that the 1D [Zn(biap)]_n chains in the *c* axis are related by translation symmetry, and those 1D chains in the *b* axis are aligned in an anti-parallel manner. The nearest Zn···Zn distance spanned by biap⁻ is 8.4485(4) Å along the *b* direction and is 8.3693(4) Å along the *c* direction. These two sets of 1D chains are crosslinked at Zn(II) nodes into a 2D puckered polymeric layer in the *bc* plane with (4,4) topology (Fig. 4b), which further interacts with each other by means of $\pi\cdots\pi$ interactions between the aromatic benzimidazole groups (centroid-to-centroid distances of 3.488 and 3.854 Å, respectively), yielding a 3D ordered supramolecular structure (Fig. 4c).

Fig. 4a is here

(a)

Fig. 4b is here

(b)

Fig. 4c is here

(c)

Fig. 4 (a) The coordination environment around Zn(II) ion in **4** (symmetry codes: A *x*, -1+*y*, *z*; B *x*, 1/2-*y*, 1/2+*z*). (b) The 2D puckered polymeric layer in the *bc* plane (left) and schematic view of

the 2D (4,4) topological network (right). Zn, teal; C, grey; N, blue; O, red. (c) Perspective diagram of the 3D framework of **4** generated *via* interlayer $\pi\cdots\pi$ stacking interactions. Hydrogen atoms are omitted for clarity.

Complex **5** belongs to the trigonal crystal system with a space group of $R\bar{3}$. Its structure reveals a nano-sized dodecanuclear Cd(II) cage bearing a garland-like shape. The discrete large cluster is a neutral species because the positive charges of twelve Cd²⁺ ions are neutralized by the negative charges of twenty-four monoanionic biap⁻ ligands. The two crystallographically independent Cd(II) ions (Cd1 and Cd2) are each coordinated in a severely twisted octahedral geometry with N₂O₄ donor atoms coming from four different biap⁻ linkers (Fig. 5a). The four ligands around a Cd(II) center are inequivalent, but all of them reveal *gauche* conformation with torsion angles of approximately $\pm 70^\circ$ about the central C–C bond. The carboxylate group of each biap⁻ chelates to one Cd(II) ion, whereas its benzimidazole N atom is connected with a second Cd(II) center (mode c), thus these tridentate ligands can be described as two-connected rods. As evident from the top view and side view of the coordination cage (Fig. 5b and 5c), one group of six Cd(II) ions locate in the upper layer of the cage, while another six lie in the lower layer. Every adjacent two of the six “upper” or “lower” metal centers are associated *via* two bent biap⁻ bridges providing three identical boat-shaped [Cd₂(biap)₂] bimetallic rings in each layer. Furthermore, two other pairs of biap⁻ linkers join each of these bimetallic species with two neighboring bimetallic ones from another layer. As a consequence, three bimetallic loops in the upper layer and another three in the lower layer are linked successively by six pairs of bridging biap⁻ into a dodecametallic cage with a hollow cavity. The intra-cage separations between two adjacent Cd ions are in the range of 6.590(1)–6.844(1) Å. From another perspective, the cage framework may be viewed as a head-to-tail 1D looped chain. Due to the chelating-bridging coordination mode of biap⁻, the bimetallic structural components of the cluster become more rigid, as confirmed by the similar dihedral angles between benzimidazole moieties of two biap⁻ ligands in two independent [Cd₂(biap)₂] rings (85.94(6)° and 80.48(7)°, respectively). The whole cage possesses 3-fold rotation symmetry with the symmetry axis passing through the central void of the cage. The size of the Cd(II) cage reaches nano-scale with an outer diameter of approximately 2.9 nm, an inner cavity diameter of about 5 Å and an architectural thickness of 1.3 nm (Fig. 5d). To the best of our

knowledge, such a novel garland-like Cd(II) nanoarchitecture is the first Cd₁₂L₂₄ type cluster reported to date, which ranks among the small family of dodecanuclear Cd(II) species as a new member.²⁴ From the difference Fourier map, a total of 1.33 lattice water molecules were assigned in the asymmetric unit. Two partially occupied disordered water molecules (O12 and O13) and their symmetry related partners are found to fill the interior cavity of the coordination cage as guest material. Another two partially occupied disordered solvent molecules (O10 and O11), water molecules positioned on the three-fold axis (O9) and their symmetry related molecules are placed around the cage and the number of water molecules per formula unit is 8. It is worthy to be mentioned that the garland-like coordination cages stack offset along the crystallographic *c* axis, so that the void of the cage should be overshadowed in the solid structure of **5** (Fig. 5e).

Fig. 5a is here

(a)

Fig. 5b is here

(b)

Fig. 5c is here

(c)

Fig. 5d is here

(d)

Fig. 5e is here

(e)

Fig. 5 (a) The coordination environments around Cd(II) ions in **5** (symmetry codes: A $-2/3+y$, $2/3-x+y$, $5/3-z$; B $4/3+x-y$, $2/3+x$, $5/3-z$). (b) Top view of [Cd₁₂(biap)₂₄] cage with garland-like appearance. Cd, teal; C, grey; N, blue; O, red. (c) Side view of the dodecanuclear Cd(II) cage emphasizing the arrangement of two groups of Cd(II) centers within the cage (green spheres represent Cd(II) in the upper layer and pink spheres represent Cd(II) in the lower layer), most C atoms of the biap⁻ ligands are omitted for clarity. (d) Space-filling picture of the cage framework looking along the 3-fold axis, showing the size and inner cavity of the nano-sized architecture with the included guest molecules being omitted. (e) Space-filling packing view of the cluster along the *c* axis, displaying the void of the cage is overshadowed through the crystal packing.

Complex **6** shows a 1D infinite wavy chain structure. The asymmetric unit consisting of two crystallographically independent Hg(II) centers. As depicted in Fig. 6a, Hg1 is tetrahedral-coordinated by two N atoms of two protonated Hbiap ligands and two Cl⁻ bridges. Hg1–N1 bond length (2.163(3) Å) and Hg1–Cl1 bond length (2.611(2) Å) fall in the expected range observed for the Hg(II)-benzimidazole complexes.²⁵ Hbiap behaves as a neutral monodentate ligand and coordinates *via* one benzimidazole N atom to Hg1 (mode b), accordingly the protonated carboxylic group is not involved in the metal ligation. Hbiap exist in this complex as an *anti* conformer with the N–C–C–C torsion angle being –155.88(37) °. Hg2 atom lies on a crystallographic inversion center and its overall geometry, made up of both terminal Cl⁻ and bridging Cl⁻ ligands, is essentially a square planar. The bond distance between Hg2 and bridging Cl2 ion (2.985(2) Å) is much longer than that between Hg2 and terminal Cl1 ligand (2.340(2) Å), however it is usual for Hg(II) complexes containing Cl⁻ bridge. Along the crystallographic *b* axis, bridging Cl⁻ groups link Hg1 and Hg2 ions alternatively to afford a 1D polymeric wavy chain (Fig. 6b), in which the nearest intra-chain Hg1···Hg2 separation *via* Cl⁻ bridge is 5.089(3) Å. Furthermore, adjacent 1D wavy chains are intercalated into each other through weak $\pi\cdots\pi$ packing interactions (centroid-to-centroid distance of 3.894 Å) between vicinal imidazole and phenyl groups, generating a 2D network along the *bc* plane (Fig. 6c). Packing of the 2D network in the crystal through the symmetric double hydrogen bonds (O2–H2C···O1 2.677(6) Å) between the uncoordinated carboxylic groups creates a 3D supramolecular framework (Fig. 6d).

Fig. 6a is here

(a)

Fig. 6b is here

(b)

Fig. 6c is here

(c)

Fig. 6d is here

(d)

Fig. 6 (a) The coordination environments around Hg(II) ions in **6** (symmetry codes: A 1–*x*, *y*, 1/2–*z*; B 1–*x*, 3–*y*, –*z*). (b) The 1D wavy coordination chain along the *c* axis sustained by Cl⁻ bridges.

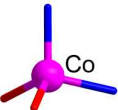
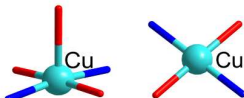
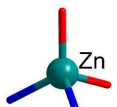
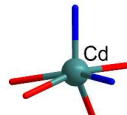
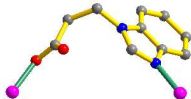
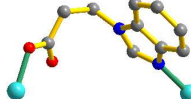
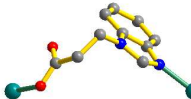
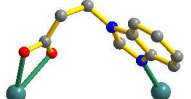
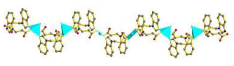
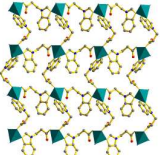
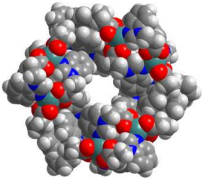
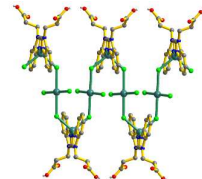
Hg, teal; C, grey; H, light grey; N, blue; O, red; Cl, bright green. (c) The 2D layered network along the *bc* plane formed by $\pi\cdots\pi$ stacking interactions. (d) The 3D supramolecular framework sustained by $\pi\cdots\pi$ interactions and O–H \cdots O hydrogen bonds. Hydrogen atoms not involved in hydrogen bonding are omitted for clarity.

Structural modulation directed by different metals

For aforementioned metal-organic complexes **1–6**, architectural transformation is observed from discrete high-nuclearity cluster, 1D polymeric chain to 2D coordination layer. At first, the conformational change of the flexible bifunctional linker is considered as the probable major factor contributing to the topological and structural alteration of the obtained complexes. But careful analysis on the structural aspects of these complexes discloses that the *anti* conformer of Hbiap/biap[–] is only present in complex **6**, and in the remaining compounds **1–5** the ligands assume *gauche* conformation with similar torsion angles. Meanwhile, the coordination architectures of complexes **1–5** differ from each other. Obviously, the conformational freedom of Hbiap might not become a key ingredient for the structural modulation in the present study. A deeper examination indicates that the preferential coordination geometries of metal centers as well as the connectivity of metal nodes are the critical factors to induce the structural change of these coordination aggregates, and the protonation status along with the binding modes of the carboxylic ligand are also non-negligible (Table 2).

Although the coordination modes and geometric conformation of the deprotonated biap[–] ligand along with the connectivity of metal nodes are identical for complexes **1**, **2** and **5**, diverse coordination geometries of the metal centers could be found in these coordination aggregates, namely tetrahedral coordinated Co(II) in **1**, square-planar or square-pyramidal coordinated Cu(II) in **2** and octahedral coordinated Cd(II) in **5**. Because the coordination geometry may further determine the spatial arrangement of the organic linkers around the metal centers, it is undoubted that the dramatic structural changes among these three complexes are mainly directed by the coordination nature of different metal ions. In **1**, each Co(II) connects to two adjacent ones by two pairs of bidentate bridges to form a 1D looped chain. The tetrahedral arrangement of four donor atoms at Co(II) does not produce remarkable steric interaction between adjacent flexible ligands.

Table 2 A summary of the structural information of metal ions and ligand in complexes 1–6

Complexes	1-Co(II)	2-Cu(II)	3-Ag(I)	4-Zn(II)	5-Cd(II)	6-Hg(II)
Metal coordination geometries	 [CoN ₂ O ₂]	 [CuN ₂ O ₃] [CuN ₂ O ₂]	 [AgN ₂]	 [ZnN ₂ O ₂]	 [CdN ₂ O ₄]	 [HgN ₂ Cl ₂] [HgCl ₄]
Hbiap/biap ⁻ binding modes and conformations	 <i>gauche</i>	 <i>gauche</i>	 <i>gauche</i>	 <i>gauche</i>	 <i>gauche</i>	 <i>anti</i>
Node's connection number	2	2	2	4	2	2
Coordination motifs	 1D looped chain	 1D undulated double-chain	 1D zigzag chain	 2D (4,4) layer	 Dodecanuclear	 1D wavy chain

It is obvious that the boat-like $[\text{Co}_2(\text{biap})_2]$ structural units of the 1D chain can be distorted to some degree with a pair of benzimidazole groups twisted to each other by different angles in two independent units. If Cu(II) cations in either square-planar or square-pyramidal sphere substitute for tetrahedral Co(II) in **1**, the N2O2 donors provided by four bridging ligands around an individual Cu(II) ion are placed in a flat plane. For the steric reason, the parallel pairs of benzimidazole moieties of ligands are oriented up and down alternatively to form a 1D undulated double-chain **2**. Within **5**, the central Cd(II) shows a severely distorted octahedral geometry and the biap^- around it adopt a chelating-bridging tridentate mode. To avoid the excessive congestion of six donor atoms around Cd(II), two ligands in each $[\text{Cd}_2(\text{biap})_2]$ ring are arranged in such a way that the benzimidazole moieties of them are nearly mutually perpendicular. Clearly, these boat-like bimetallic ring become more rigid in contrast to the $[\text{Co}_2(\text{biap})_2]$ dimer. Fortunately, $[\text{Cd}_2(\text{biap})_2]$ loops are then interlinked together to yield a discrete garland-like coordination cage. In complex **3**, di-coordinated Ag(I) is bound by two partially deprotonated ligands to give a $[\text{Ag}(\text{H}_{0.5}\text{biap})_2]$ unit, which is coupled with each other by specific $\text{O}\cdots\text{H}\cdots\text{O}$ interaction yielding a 1D zigzag chain. Zn(II) center in **4** reveals a four-coordinated tetrahedral geometry as Co(II) center in **1**, but the connectivity between the metal nodes are totally different in these two complexes. Each Zn(II) as a four-connected node is in conjunction with its four partners *via* four biap^- , leading to the dimension transformation from 1D chain to 2D (4,4) sheet. Different from the above complexes, simple anion Cl^- in place of protonated Hbiap acts as a connector to join both tetrahedral and square-planar Hg(II) centers into a 1D infinite wavy chain **6**.

Thermogravimetric analysis

The thermogravimetric analyses (TGA) were conducted on the polycrystalline samples of complexes **1–5** to investigate their pyrolytic characteristics under N_2 atmosphere (Fig. S2). For complexes **2**, **3** and **5** containing lattice water and/or coordinated water molecules, three well-defined thermal degradation stages could be observed in their TGA curves. The first weight loss, in the temperature range of 30–150 °C, is the result of the removal of all lattice and coordinated water molecules from the complex molecules (for **2**, obsd: 14.06% and calcd: 14.02%; for **3**, obsd: 7.80% and calcd: 6.89%; for **5**, obsd: 2.06% and calcd: 2.31%). The deviation of the observed value from the calculated value for **3** probably arises from the presence of a small

amount of adsorbed water on the sample surface. Afterwards, the second weight decrease of 32.68%, 57.23% and 28.79% from 190 to 300, 160 to 280 and 240 to 400 °C for **2**, **3** and **5**, respectively, is either in consistent with the departure of the $\text{CH}_2\text{CH}_2\text{COO}^-$ moiety from the biap^{16a} ligand in **2** and **5** (calcd 28.06% for **2** and 29.44% for **5**) or due to the destroy of part of the organic ligand in **3**. The third decomposition step is observed between 340 and 370 °C for **2**, 380 and 470 for **3** and 400 and 490 °C for **5**, ascribed to the complete combustion of the heterocyclic fragments. At the end of the third stage, only corresponding metal oxides or non-volatile metal element are left as residues (CuO for **2**, obsd: 16.96% and calcd: 15.48%; Ag for **3**, obsd: 23.41% and calcd: 20.61 %; CdO for **5**, obsd: 22.14% and calcd: 25.45%).

As a comparison, the non-hydrated complexes **1** and **4** only show two thermal decomposition steps in the temperature range of 30–800 °C. The initial step observed between 280 and 360 °C for **1** and between 300 and 470 °C for **4**, corresponds to the elimination of the $\text{CH}_2\text{CH}_2\text{COO}^-$ functionality from the bifunctional ligand (obsd: 30.21%, 32.18% and calcd: 32.96%, 32.48% for complexes **1** and **4**, respectively). Subsequently, the second combustion step starts immediately following the first one and stops at 380 °C for **1** or 515 °C for **4**, attributed to the further degradation of the remaining organic components.

Luminescence spectroscopy

The solid-state photoluminescence properties of the heterocyclic organic linker and its four complexes **3–6** containing d^{10} transition metal centers were determined under room temperature. The normalized excited and emission spectra are shown in Fig.S3 and 7. Ligand Hbiap and complexes **4** and **5** display excitation bands between 240–310 nm, whereas the excitation spectra of complexes **3** and **6** have maxima at 368 and 399 nm, respectively. Upon excited by a UV light at 283 nm, the free ligand Hbiap shows an emission peak centered around 303 nm, corresponding to the π - π^* transitions of the aromatic benzimidazole moiety. The luminescent emission profiles of complexes **4** and **5** resemble to that of the original ligand with the maximum peaks at about 333 nm ($\lambda_{\text{ex}} = 290$ nm) and 325 nm ($\lambda_{\text{ex}} = 291$ nm), respectively, therefore these emission spectra are essentially intraligand π - π^* transitions. The luminescent complexes **3** and **6** produce similar emission peaks shifting towards longer wavelengths apparently with respect to those observed for

4 and **5**. The emission maxima are found at 440 nm ($\lambda_{\text{ex}} = 368$ nm) for **3** and 464 nm ($\lambda_{\text{ex}} = 399$ nm) for **6**. We could tentatively define these emissions as the ligand to metal charge transfer transition (LMCT) instead of the ligand based transition.²⁶ The discrepancy of the luminescence properties between the former two complexes (**4** and **5**) and the latter ones (**3** and **6**) could be attributed to the varied coordination modes ranging from μ_2 -bridging to monodentate adopted by the organic ligand in the above complexes.

Fig. 7 is here

Fig. 7 The normalized solid-state photoluminescent emission spectra of ligand Hbiap and complexes **3–6** at room temperature.

Conclusions

In summary, five low-dimensional coordination polymers and a novel discrete dodecametallic cage have been obtained from appropriate transition metals in combination with a flexible bifunctional benzimidazole carboxylic acid. The coordination numbers and geometries of central metals along with the connectivity of metal ions are related to the structural diversification of the resultant complexes. The high-nuclearity Cd(II) cage presents a garland-like appearance and possesses a typical hydrophobic cavity. Our continuous investigations attempt to make use of N-containing heterocycles attached with carboxylic acids having longer alkyl chains to acquire high-nuclearity metal-organic cages with tunable pore size and find their potential applications in molecular recognition and separation.

Acknowledgements

This work is financially supported by the Natural Science Foundation of China (grant No. 21361004), Guangxi Natural Science Foundation of China (grant No. 2014GXNSFAA118044) and the Key Laboratory for the Chemistry and Molecular Engineering of Medicinal Resources (Guangxi Normal University), Ministry of Education of China (CMEMR 2012-A08, CMEMR 2013-C08).

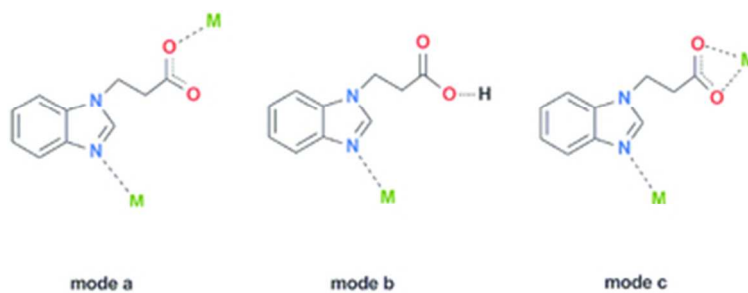
Notes and References

- 1 (a) H. Furukawa, K. E. Cordova, M. O'Keeffe and O. M. Yaghi, *Science*, 2013, **341**, 974; (b) W. Lu, Z. Wei, Z.-Y. Gu, T.-F. Liu, J. Park, J. Park, J. Tian, M. Zhang, Q. Zhang, T. Gentle III, M. Bosch and H.-C. Zhou, *Chem. Soc. Rev.*, 2014, **43**, 5561; (c) S. Qiu and G. Zhu, *Coord. Chem. Rev.*, 2009, **253**, 2891; (d) M. L. Foo, R. Matsuda and S. Kitagawa, *Chem. Mater.*, 2014, **26**, 310.
- 2 (a) D. Zhao, D. J. Timmons, D. Yuan and H.-C. Zhou, *Acc. Chem. Res.*, 2011, **44**, 123; (b) F. A. A. Paz, J. Klinowski, S. M. F. Vilela, J. P. C. Tomé, J. A. S. Cavaleiro and J. Rocha, *Chem. Soc. Rev.*, 2012, **41**, 1088; (c) M. J. Prakash and M. S. Lah, *Chem. Commun.*, 2009, **23**, 3326; (d) J. Wang, Y.-H. Zhang and M.-L. Tong, *Chem. Commun.*, 2006, **30**, 3166; (e) X. Zhou, B. Li, G. Li, Q. Zhou, Z. Shi and S. Feng, *CrystEngComm*, 2012, **14**, 4664.
- 3 (a) Y. Yao, Y. Che and J. Zheng, *Cryst. Growth Des.*, 2008, **8**, 2299; (b) S.-R. Zheng, S.-L. Cai, J. Fan, T.-T. Xiao and W.-G. Zhang, *Inorg. Chem. Commun.*, 2011, **14**, 818; (c) S. Wang, T. Zhao, G. Li, L. Wojtas, Q. Huo, M. Eddaoudi and Y. Liu, *J. Am. Chem. Soc.*, 2010, **132**, 18038; (d) Y. Liu, V. Ch. Kravtsov and M. Eddaoudi, *Angew. Chem. Int. Edit.*, 2008, **47**, 8446; (e) C. S. Hawes, and P. E. Kruger, *RSC Adv.*, 2014, **4**, 15770; (f) B. Tu, Q. Pang, D. Wu, Y. Song, L. Weng and Q. Li, *J. Am. Chem. Soc.*, 2014, **136**, 14465; (g) V. Safarifard and A. Morsali, *CrystEngComm*, 2011, **13**, 4817; (h) W. Zheng, Y. Wei, X. Xiao and K. Wu, *Dalton Trans.*, 2012, 3138; (i) A. Rodriguez-Dieguez, A. J. Mota, J. Cano, J. Ruiz, D. Choquesillo-Lazarte and E. Colacio, *Dalton Trans.*, 2009, 6335; (j) Y.-F. Yue, J. Liang, E.-Q. Gao, C.-J. Fang, Z.-G. Yan and C.-H. Yan, *Inorg. Chem.*, 2008, **47**, 6115.
- 4 (a) Z. Xia, Q. Wei, Q. Yang, C. Qiao, S. Chen, G. Xie, G. Zhang, C. Zhou and S. Gao, *CrystEngComm*, 2013, **15**, 86; (b) X.-J. Hong, M.-F. Wang, H.-G. Jin, Q.-G. Zhan, Y.-T. Liu, H.-Y. Jia, X. Liu and Y.-P. Cai, *CrystEngComm*, 2013, **15**, 5606; (c) A. Ablet, S.-M. Li, W. Cao, X.-J. Zheng, W.-T. Wong and L.-P. Jin, *Chem. Asian J.*, 2013, **8**, 95; (d) M.-F. Wu, F.-K. Zheng, A.-Q. Wu, Y. Li, M.-S. Wang, W.-W. Zhou, F. Chen, G.-C. Guo and J.-S. Huang, *CrystEngComm*, 2010, **12**, 260; (e) B. Ding, E.-C. Yang, J.-H. Guo, X.-J. Zhao and X.-G. Wang, *Inorg. Chem. Commun.*, 2008, **11**, 1481; (f) Z. Zhang, S. Xiang, Q. Zheng, X. Rao, J. U. Mondal, H. D. Arman, G. Qian and B. Chen, *Cryst. Growth Des.*, 2010, **10**, 2372.

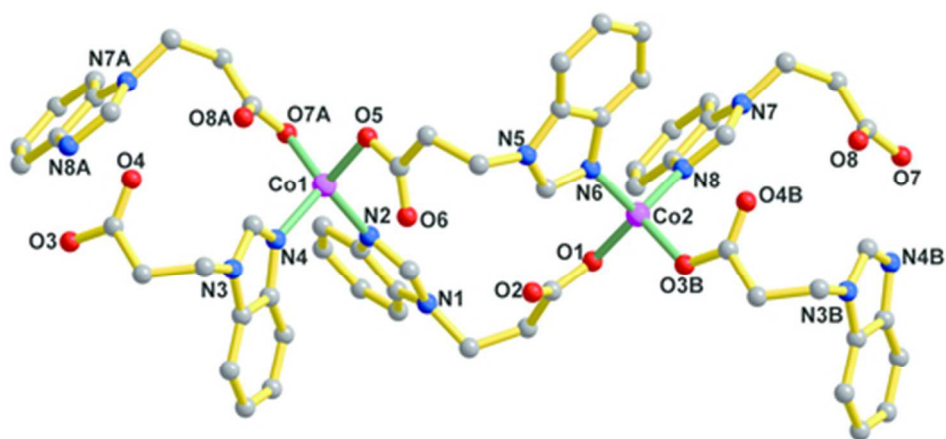
- 5 (a) Q. Xu, R.-Q. Zou, R.-Q. Zhong, C. Kachi-Terajima and S. Takamizawa, *Cryst. Growth Des.*, 2008, **8**, 2458; (b) M. Wriedt, A. A. Yakovenko, G. J. Halder, A. V. Prosvirin, K. R. Dunbar and H.-C. Zhou, *J. Am. Chem. Soc.*, 2013, **135**, 4040; (c) Y.-G. Sun, G. Xiong, M.-Y. Guo, F. Ding, S.-J. Wang, P. F. Smet, D. Poelman, E.-J. Gao and F. Verpoort, *Dalton Trans.*, 2012, 7670; (d) Q. Ma, M. Zhu, L. Lu, S. Feng and T. Wang, *Dalton Trans.*, 2010, 5877.
- 6 (a) K. Jayaramulu, S. K. Reddy, A. Hazra, S. Balasubramanian and T. K. Maji, *Inorg. Chem.*, 2012, **51**, 7103; (b) Z.-G. Gu, Y.-T. Liu, X.-J. Hong, Q.-G. Zhan, Z.-P. Zheng, S.-R. Zheng, W.-S. Li, S.-J. Hu and Y.-P. Cai, *Cryst. Growth Des.*, 2012, **12**, 2178; (c) T. K. Maji, G. Mostafa, H.-C. Chang and S. Kitagawa, *Chem. Commun.*, 2005, 2436; (d) H.-R. Fu and J. Zhang, *Cryst. Growth Des.*, 2015, **15**, 1210; (e) T.-W. Tseng, T.-T. Luo, S.-Y. Chen, C.-C. Su, K.-M. Chi and K.-L. Lu, *Cryst. Growth Des.*, 2013, **13**, 510.
- 7 (a) E. Quartapelle Procopio, F. Linares, C. Montoro, V. Colombo, A. Maspero, E. Barea and J. A. R. Navarro, *Angew. Chem. Int. Edit.*, 2010, **49**, 7308; (b) A. Kilic, C. Atalay-Oral, A. Sirkecioglu, S. B. Tantekin-Ersolmaz and M. G. Ahunbay, *J. Membrane Sci.*, 2015, **489**, 81.
- 8 (a) L. Zhang, L. Wang, P.-C. Wang, T. Song, D. Li, X. Chen, Y. Fan and J. Xu, *Eur. J. Inorg. Chem.*, 2015, 931; (b) G. Süß-Fink, S. Stanislas, G. B. Shul'pin, G. V. Nizova, H. Stoeckli-Evans, A. Neels, C. Bobillier and S. Claude, *J. Chem. Soc. Dalton Trans.*, 1999, 3169; (c) R.-Q. Zou, H. Sakurai, Q. Xu, *Angew. Chem. Int. Edit.*, 2006, **45**, 2542.
- 9 (a) Q.-G. Zhai, C. Mao, X. Zhao, Q. Lin, F. Bu, X. Chen, X. Bu and P. Feng, *Angew. Chem. Int. Edit.*, 2015, **54**, 7886; (b) X. Zhao, C. Mao, X. Bu and P. Feng, *Chem. Mater.*, 2014, **26**, 2492.
- 10 (a) T.-F. Liu, J. Lü and R. Cao, *CrystEngComm*, 2010, **12**, 660; (b) J.-R. Li and X.-H. Bu, *Eur. J. Inorg. Chem.* 2008, 27; (c) G.-Q. Kong and C.-D. Wu, *CrystEngComm*, 2012, **14**, 847; (d) X.-J. Wang, Z.-M. Cen, Q.-L. Ni, X.-F. Jiang, H.-C. Lian, L.-C. Gui, H.-H. Zuo and Z.-Y. Wang, *Cryst. Growth Des.*, 2010, **10**, 2960; (e) M.-X. Yao, M.-H. Zeng, H.-H. Zou, Y.-L. Zhou and H. Liang, *Dalton Trans.*, 2008, 2428; (f) S.-R. Zheng, S.-L. Cai, J.-B. Tan, J. Fan and W.-G. Zhang, *Inorg. Chem. Commun.*, 2012, **21**, 100.
- 11 (a) T.-L. Hu, W.-P. Du, B.-W. Hu, J.-R. Li, X.-H. Bu and R. Cao, *CrystEngComm*, 2008, **10**, 1037; (b) B.-W. Hu, J.-P. Zhao, Q. Yang, F.-C. Liu, X.-H. Bu, *J. Mater. Chem.*, 2009, **19**, 6827; (c) B.-W. Hu, J.-P. Zhao, Q. Yang, T.-L. Hu, W.-P. Du and X.-H. Bu, *J. Solid State Chem.*, 2009,

- 182**, 2918; (d) Y.-T. Wang, G.-M. Tang, Y.-Q. Wei, T.-X. Qin, T.-D. Li, J.-B. Ling and X.-F. Long, *Inorg. Chem. Commun.*, 2009, **12**, 1164; (e) H.-X. Chen, X.-P. Xu, Q.-F. Xu, Y. Zhang, H. Li, N.-J. Li, B. Wu and J.-M. Lu, *Polyhedron*, 2012, **41**, 77; (f) X.-Y. Chen, G. S. Goff, B. L. Scott, M. T. Janicke and W. Runde, *Inorg. Chem.*, 2013, **52**, 3217; (g) D.-G. Ding, L.-X. Xie, Y.-T. Fan, H.-W. Hou and Y. Xu, *J. Solid State Chem.*, 2009, **182**, 1443; (h) H. Yang, L. Li, J. Wu, H. Hou, B. Xiao and Y. Fan, *Chem. Eur. J.*, 2009, **15**, 4049; (i) W.-W. Dong, J. Zhao and L. Xu, *Cryst. Growth Des.*, 2008, **8**, 2882.
- 12 (a) J.-H. Wang, G.-M. Tang, Y.-T. Wang, T.-X. Qin and S. W. Ng, *CrystEngComm*, 2014, **16**, 2660; (b) Y.-T. Wang, G.-M. Tang and D.-W. Qin, *Aust. J. Chem.*, 2006, **59**, 647; (c) X.-Y. Zhou, Y.-Q. Huang and W.-Y. Sun, *Inorg. Chim. Acta*, 2009, **362**, 1399; (d) J.-H. Wang, G.-M. Tang, T.-X. Qin, S.-C. Yan, Y.-T. Wang, Y.-Z. Cui and S. W. Ng, *J. Solid State Chem.*, 2014, **219**, 55.
- 13 (a) F. He, M.-L. Tong, X.-L. Yu and X.-M. Chen, *Inorg. Chem.*, 2005, **44**, 559; (b) Q. Yu, X.-Q. Zhang, H.-D. Bian, H. Liang, B. Zhao, S.-P. Yan and D.-Z. Liao, *Cryst. Growth. Des.*, 2008, **8**, 1140; (c) L. Chen, H.-Y. Jia, X.-J. Hong, D.-H. Chen, Z.-P. Zheng, H.-G. Jin, Z.-G. Gu and Y.-P. Cai, *Inorg. Chem. Commun.*, 2013, **27**, 22.
- 14 (a) D.-G. Ding, H. Xu, Y.-T. Fan and H.-W. Hou, *Inorg. Chem. Commun.*, 2008, **11**, 1280; (b) J. Chen, S.-H. Wang, Z.-F. Liu, M.-F. Wu, Y. Xiao, F.-K. Zheng, G.-C. Guo and J.-S. Huang, *New J. Chem.*, 2014, **38**, 269.
- 15 J. Chen, S.-H. Wang, Z.-F. Liu, M.-F. Wu, Y. Xiao, R. Li, F.-K. Zheng and G.-C. Guo, *Inorg. Chem. Commun.*, 2014, **46**, 207.
- 16 (a) Z. Zhang, D.-F. Wu, K. Hu, Y.-J. Shi, Z.-L. Chen and F.-P. Liang, *J. Coord. Chem.*, 2013, **66**, 2499; (b) Z. Zhang, K. Hu, Y.-J. Shi, J.-M. Qin, Z.-L. Chen and F.-P. Liang, *Transition Met. Chem.*, 2013, **38**, 327.
- 17 N. K. Khakimova, A. A. Shazhenov and Ch. Sh. Kadyrov, *Dokl. Akad. Nauk UzSSR*, 1975, **32**, 35.
- 18 G. M. Sheldrick, *SADABS: Program for Empirical Absorption Correction of Area Detector Data*, University of Göttingen, Germany, 1996.
- 19 Bruker AXS, *SAINT Software Reference Manual*, Madison, WI, 1998.

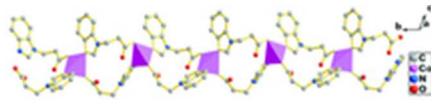
- 20 G. M. Sheldrick, *SHELXTL NT Version 5.1. Program for Solution and Refinement of Crystal Structures*, University of Göttingen, Germany, 1997.
- 21 Y. Liu, M. Pan, K. Li, C. Yan, Y. Shen, C.-Y. Zhao, W. Wang and C.-Y. Su, *Cryst. Growth Des.*, 2011, **11**, 4876.
- 22 (a) M. Arıcı, O. Z. Yeşilel and M. Taş, *Dalton Trans.*, 2015, 1627; (b) J. Y. Wu, C. W. Yang, H. F. Chen, Y. C. Jao, S. M. Huang, T. W. Tseng, G. H. Lee, S. M. Peng and K. L. Lu, *J. Solid State Chem.*, 2011, **184**, 1740.
- 23 (a) I. M. Müller, R. Robson and F. Separovic, *Angew. Chem. Int. Ed.*, 2001, **40**, 4385; (b) N. K. Al-Rasbi, I. S. Tidmarsh, S. P. Argent, H. Adams, L. P. Harding and M. D. Ward, *J. Am. Chem. Soc.*, 2008, **130**, 11641; (c) I. A. Riddell, T. K. Ronson, J. K. Clegg, C. S. Wood, R. A. Bilbeisi and J. R. Nitschke, *J. Am. Chem. Soc.*, 2014, **136**, 9491; (d) K.-C. Sham, S.-M. Yiu and H.-L. Kwong, *Inorg. Chem.*, 2013, **52**, 5648.
- 24 H.-Y. Liu, J.-F. Ma, Y.-Y. Liu, J. Yang, *CrystEngComm*, 2013, **15**, 2699.
- 25 (a) S.-R. Zheng, Q.-Y. Yang, R. Yang, M. Pan, R. Cao, and C.-Y. Su, *Cryst. Growth Des.*, 2009, **9**, 2341; (b) X.-P. Li, J.-Y. Zhang, Y. Liu, M. Pan, S.-R. Zheng, B.-S. Kang and C.-Y. Su, *Inorg. Chim. Acta*, 2007, **360**, 2990.
- 26 (a) M. D. Allendorf, C. A. Bauer, R. K. Bhakta and R. J. T. Houk, *Chem. Soc. Rev.*, 2009, **38**, 1330; (b) S.-L. Li, Y.-Q. Lan, J.-C. Ma, J.-F. Ma and Z.-M. Su, *Cryst. Growth Des.*, 2010, **10**, 1161.



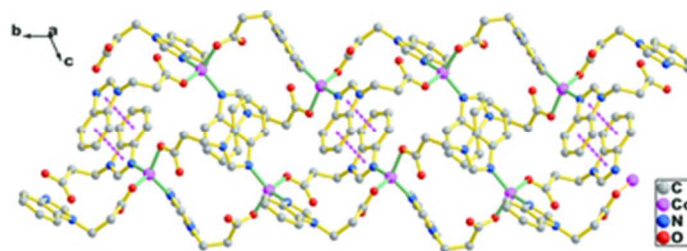
Three coordination modes of ligand Hbiap observed in complexes 1–6.
31x12mm (300 x 300 DPI)



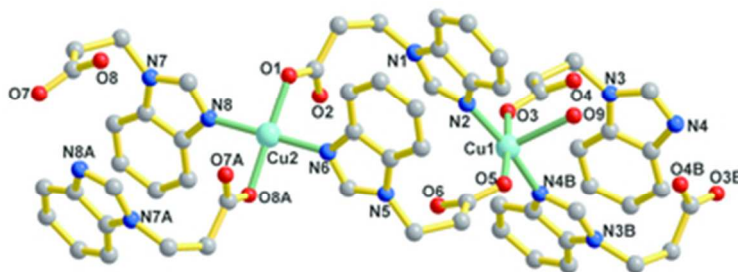
The coordination environments around Co(II) ions in **1** (symmetry codes: A $x, 1+y, z$; B $x, -1+y, z$).
40x19mm (300 x 300 DPI)



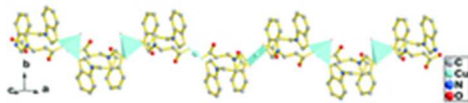
View of the 1D looped chain extending along the b axis. Co, pink; C, grey; N, blue; O, red.
18x3mm (300 x 300 DPI)



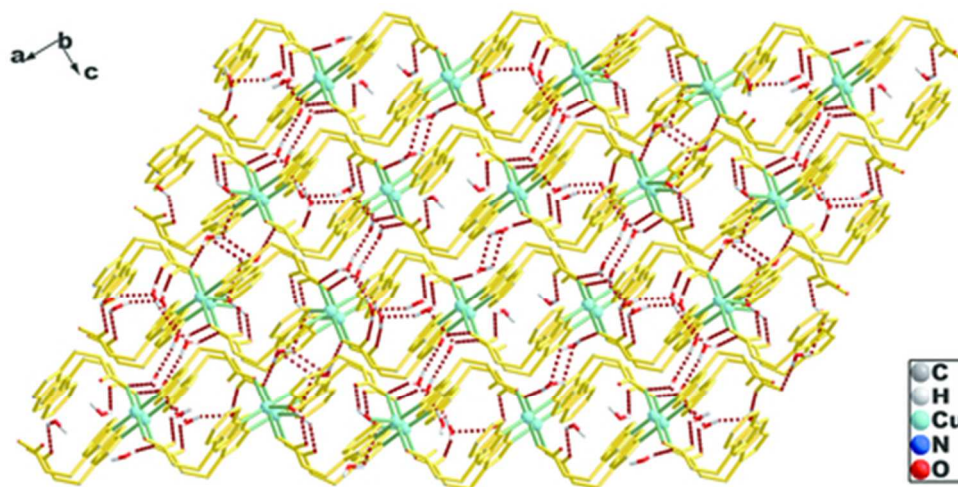
Two 1D looped chains are joined by interchain n...n stacking interactions into a double chain aggregate.
Hydrogen atoms are omitted for clarity.
29x10mm (300 x 300 DPI)



The coordination environments around Cu(II) ions in **2** (symmetry codes: A $-x, y, 3/2-z$; B $1-x, y, 1/2-z$).
31x12mm (300 x 300 DPI)



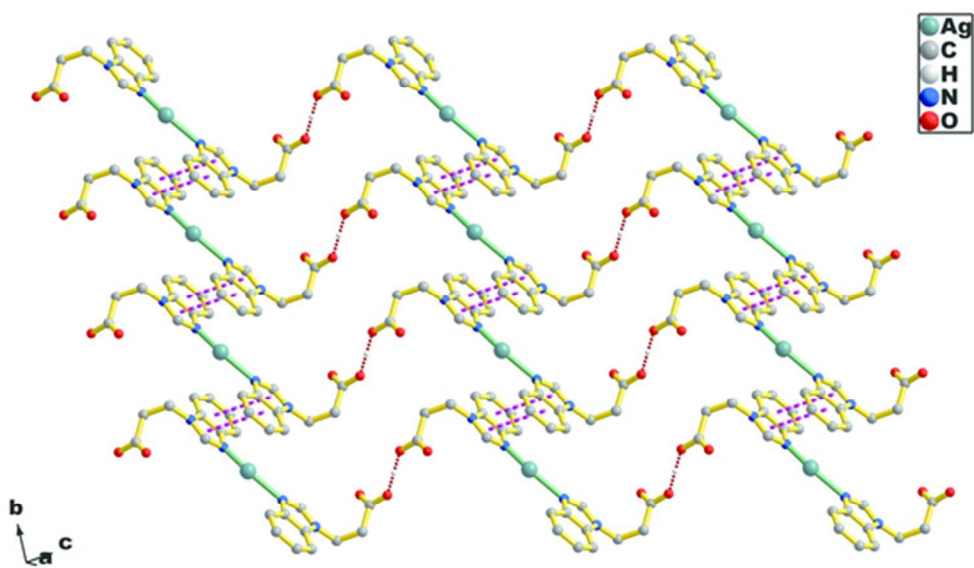
The 1D undulated double-chain of 2. Cu, aqua; C, grey; N, blue; O, red.
19x4mm (300 x 300 DPI)



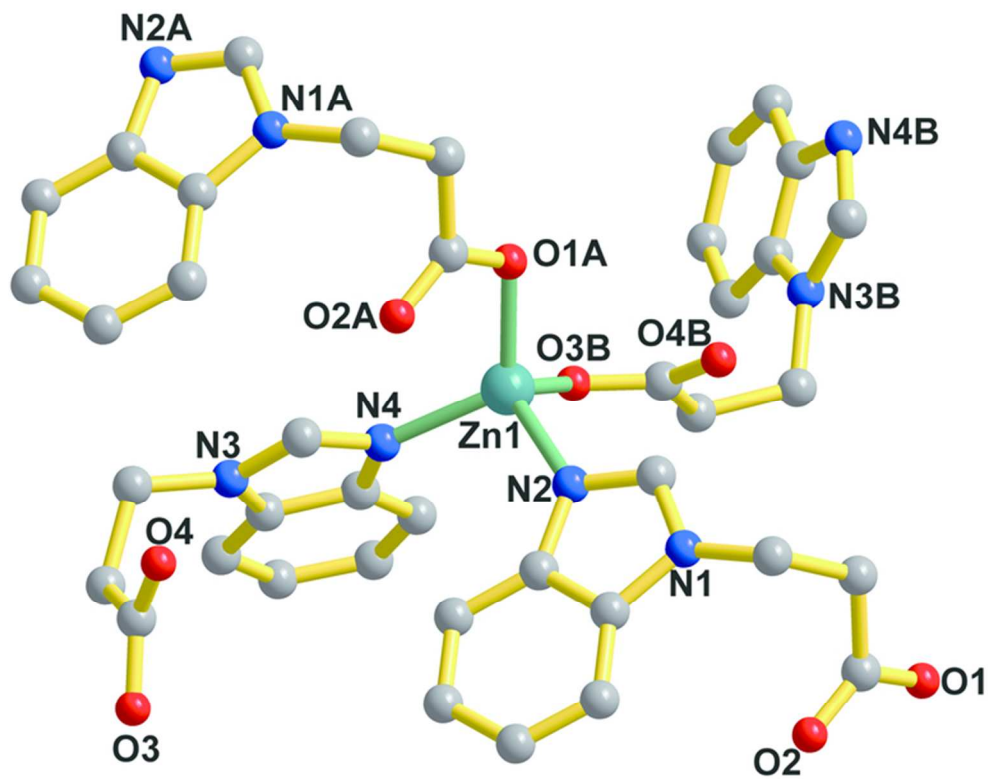
The 3D supramolecular framework formed by O-H...O hydrogen bonds. Hydrogen atoms not involved in hydrogen bonding are omitted for clarity.
41x20mm (300 x 300 DPI)



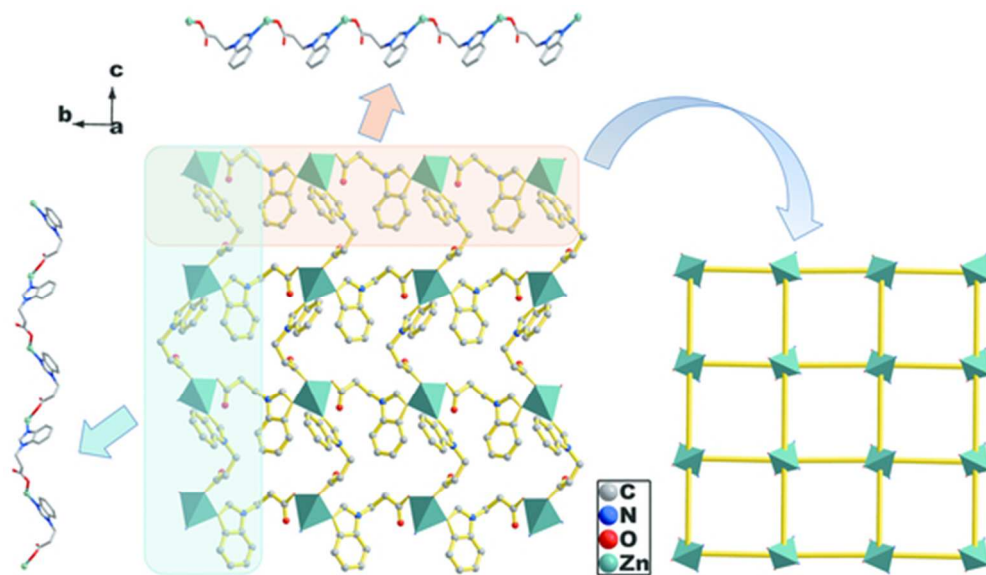
The 1D zigzag chain formed by O...H...O interactions viewed along the a direction. Ag, aqua; C, grey; H, light grey; N, blue; O, red.
15x2mm (300 x 300 DPI)



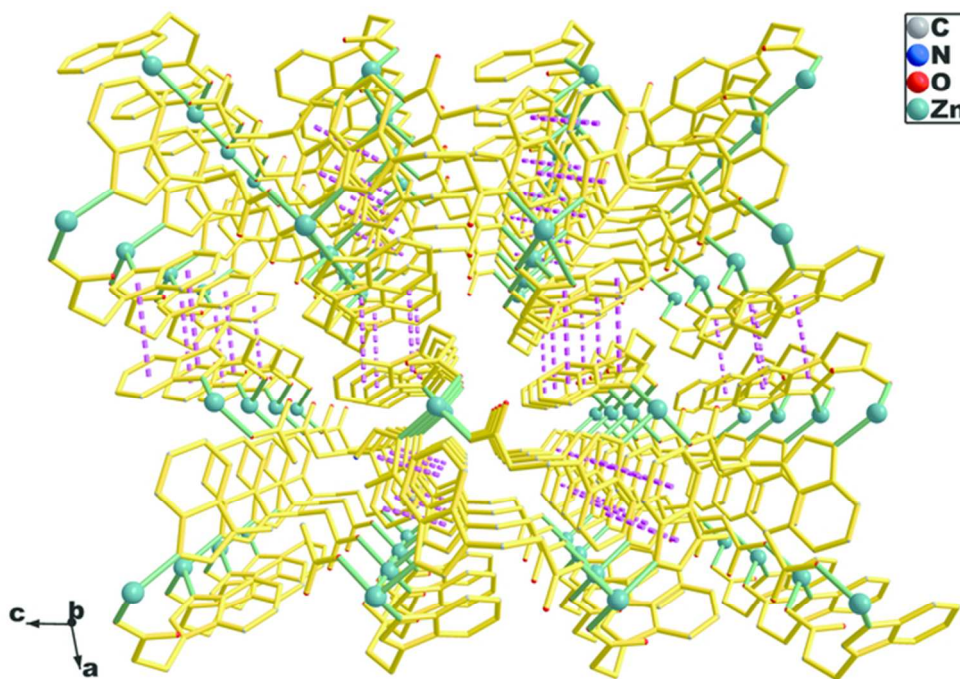
The 2D sheet sustained by interchain $n \cdots n$ stacking interactions. All solvent molecules and hydrogen atoms not involved in $O \cdots H \cdots O$ interactions are omitted for clarity.
51x32mm (300 x 300 DPI)



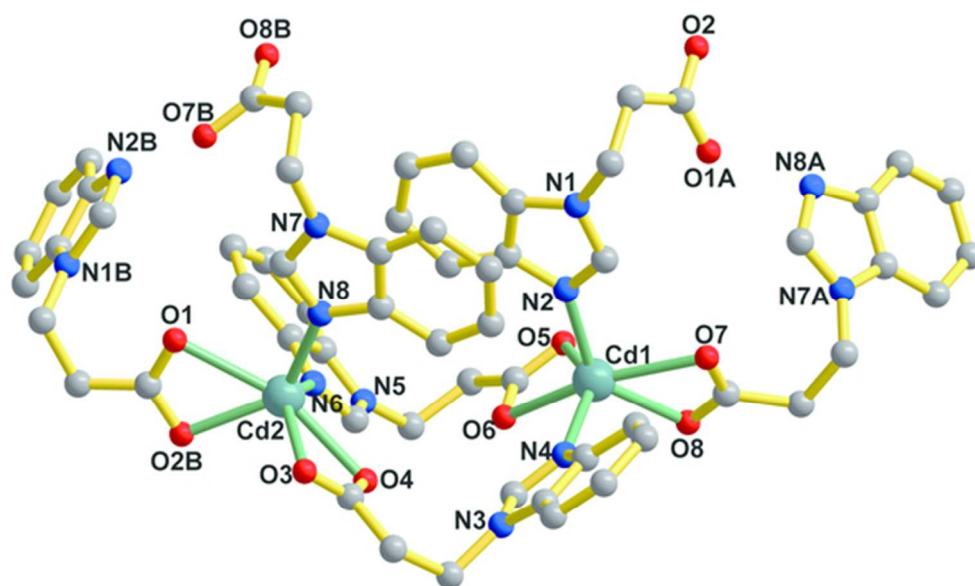
The coordination environment around Zn(II) ion in **4** (symmetry codes: A $x, -1+y, z$; B $x, 1/2-y, 1/2+z$).
66x53mm (300 x 300 DPI)



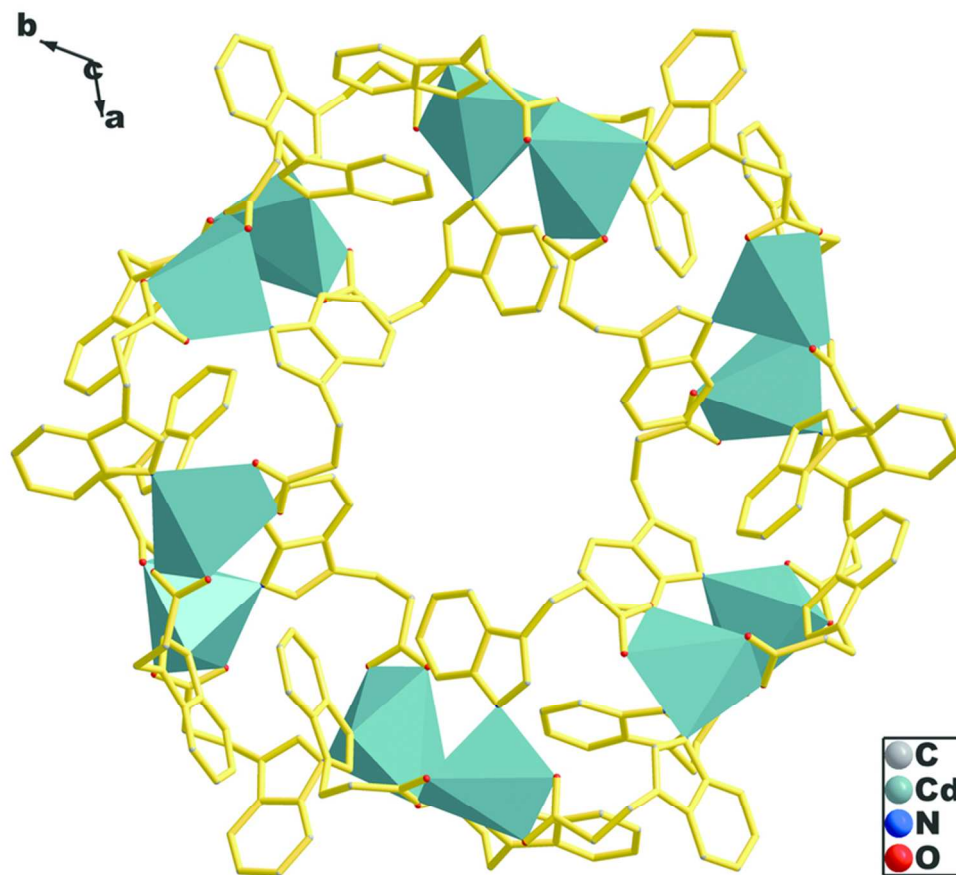
The 2D puckerd polymeric layer in the bc plane (left) and schematic view of the 2D (4,4) topological network (right). Zn, teal; C, grey; N, blue; O, red.
48x28mm (300 x 300 DPI)



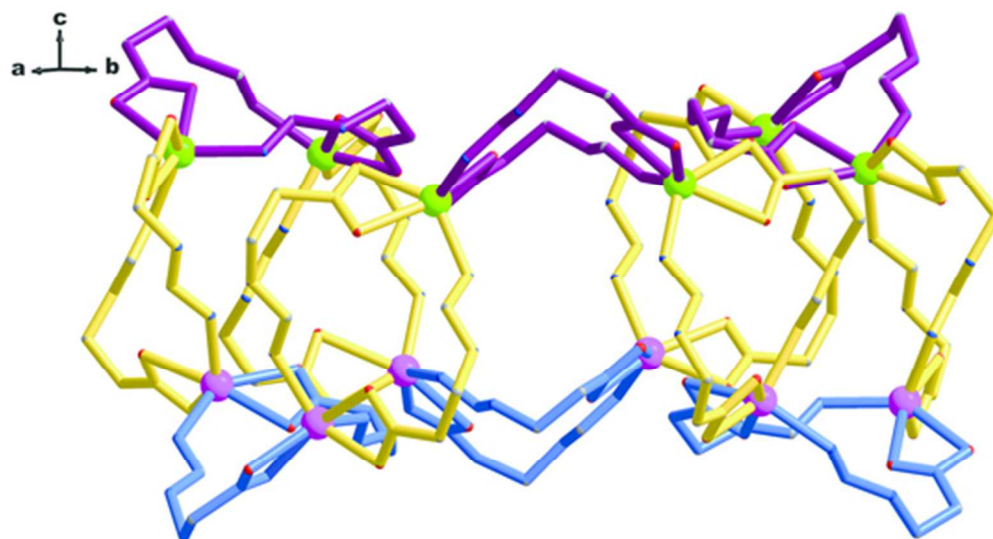
Perspective diagram of the 3D framework of **4** generated via interlayer $\pi \cdots \pi$ stacking interactions. Hydrogen atoms are omitted for clarity.
59x43mm (300 x 300 DPI)



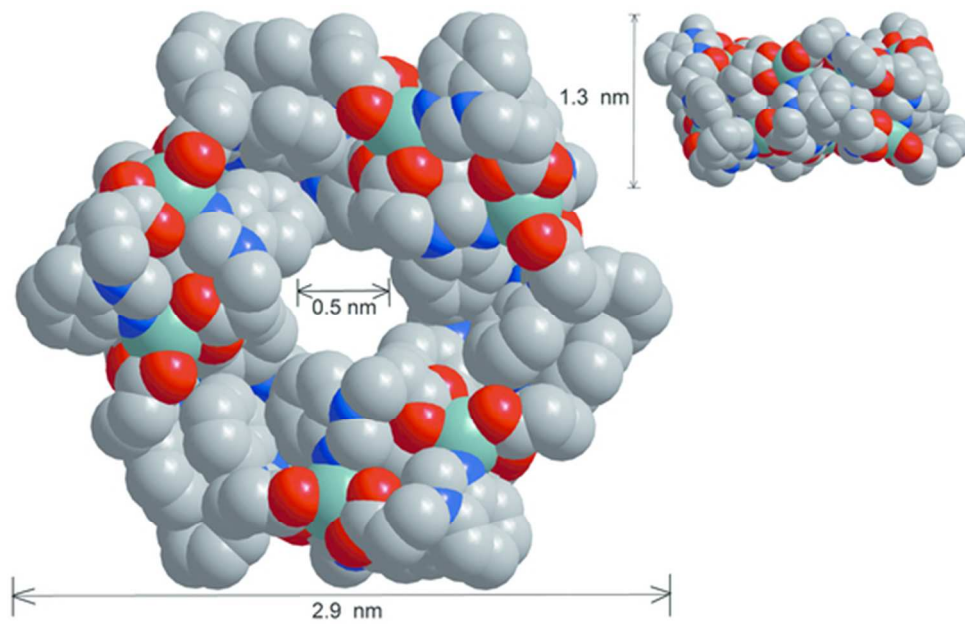
The coordination environments around Cd(II) ions in 5 (symmetry codes: A $-2/3+y, 2/3-x+y, 5/3-z$; B $4/3+x-y, 2/3+x, 5/3-z$).
51x32mm (300 x 300 DPI)



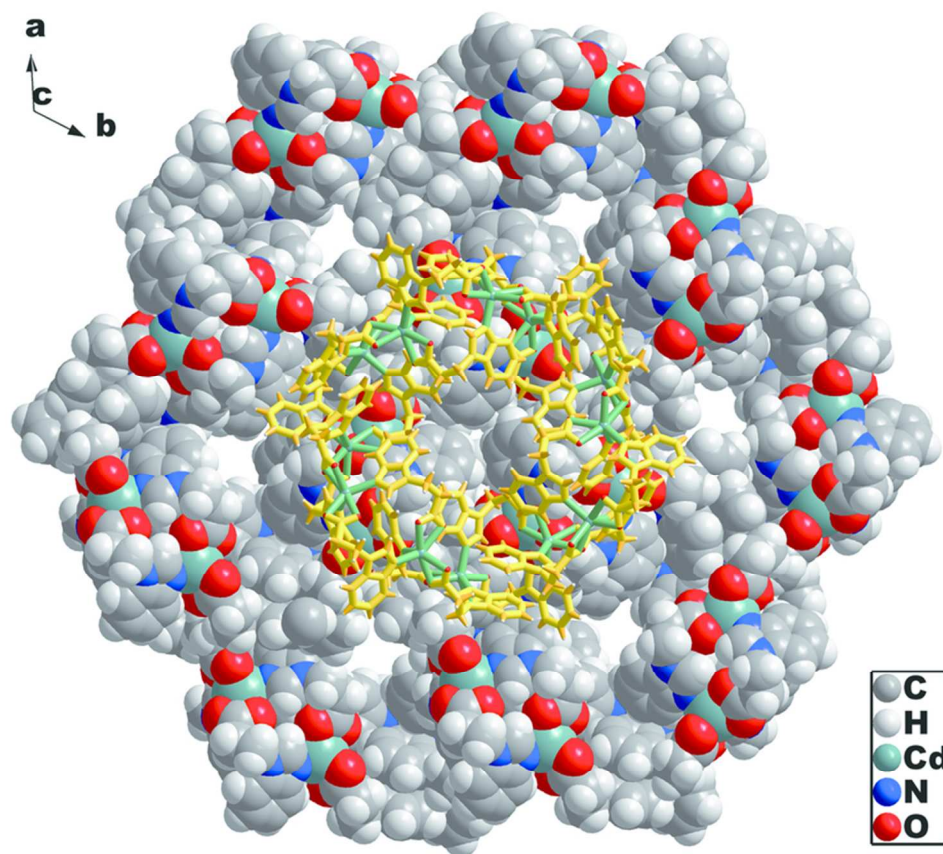
Top view of [Cd₁₂(biap)₂₄] cage with garland-like appearance. Cd, teal; C, grey; N, blue; O, red.
75x67mm (300 x 300 DPI)



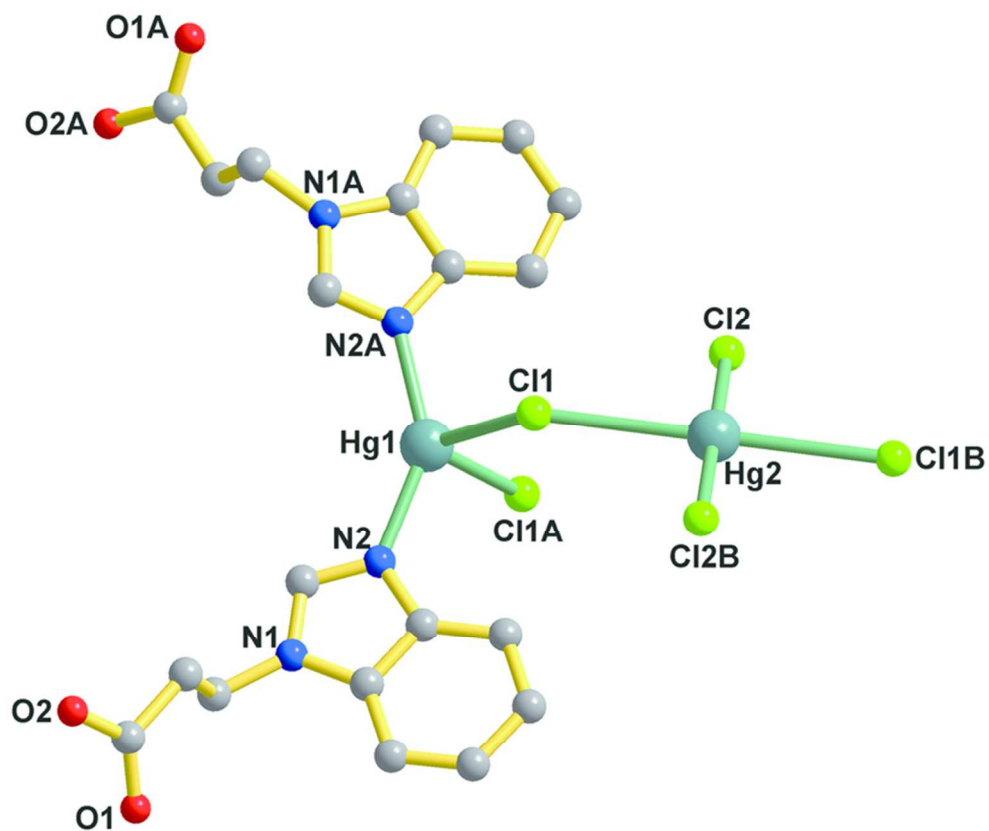
Side view of the dodecanuclear Cd(II) cage emphasizing the arrangement of two groups of Cd(II) centers within the cage (green spheres represent Cd(II) in the upper layer and pink spheres represent Cd(II) in the lower layer), most C atoms of the biap- ligands are omitted for clarity.
45x25mm (300 x 300 DPI)



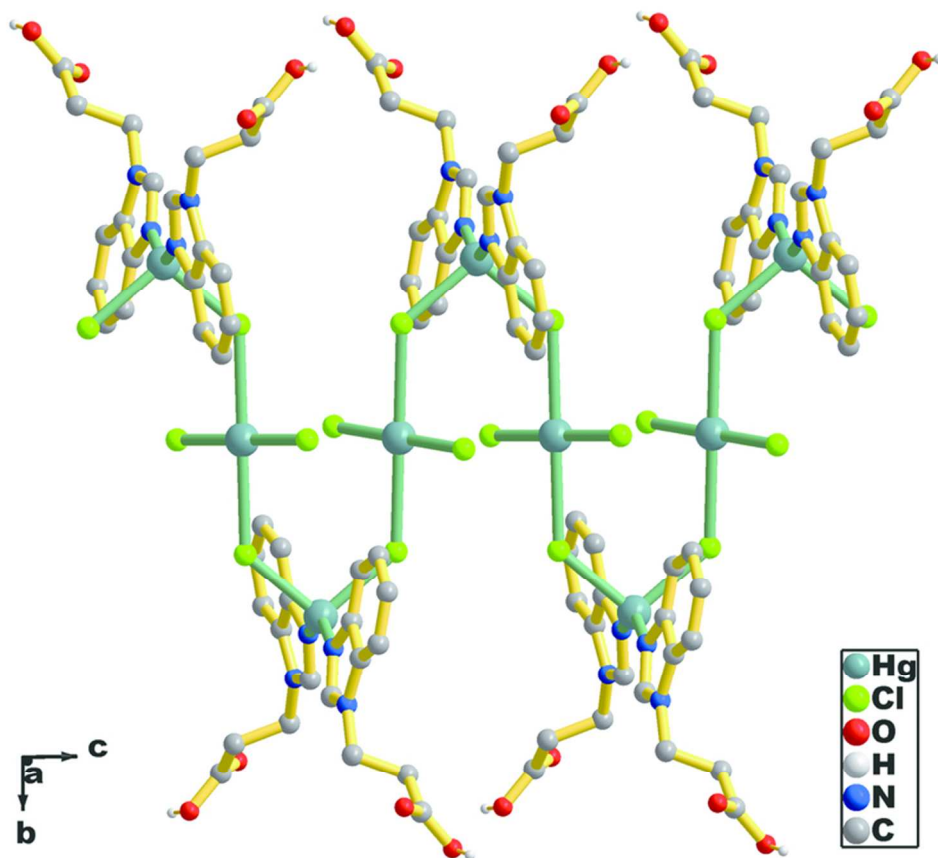
Space-filling picture of the cage framework looking along the 3-fold axis, showing the size and inner cavity of the nano-sized architecture with the included guest molecules being omitted.
51x31mm (300 x 300 DPI)



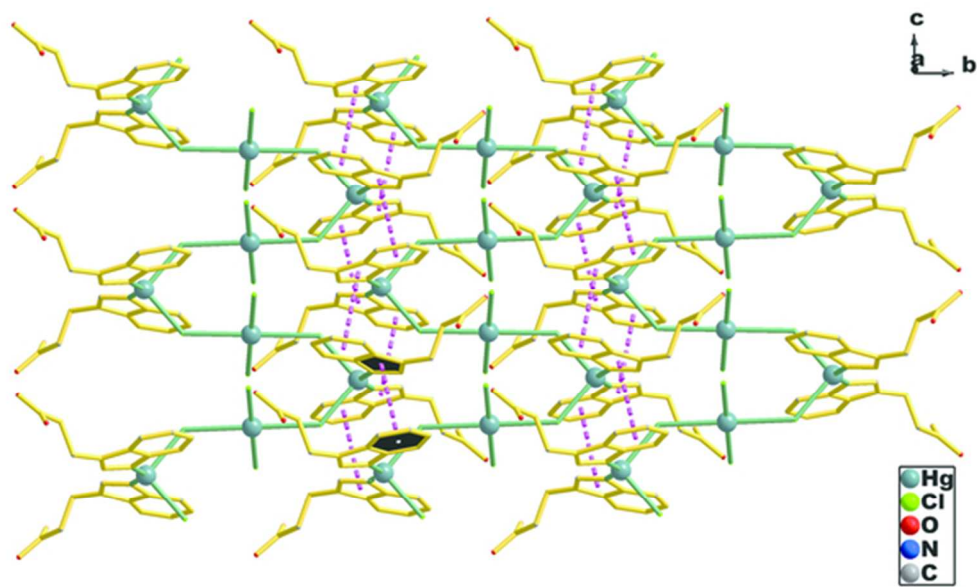
Space-filling packing view of the cluster along the c axis, displaying the void of the cage is overshadowed through the crystal packing.
73x65mm (300 x 300 DPI)



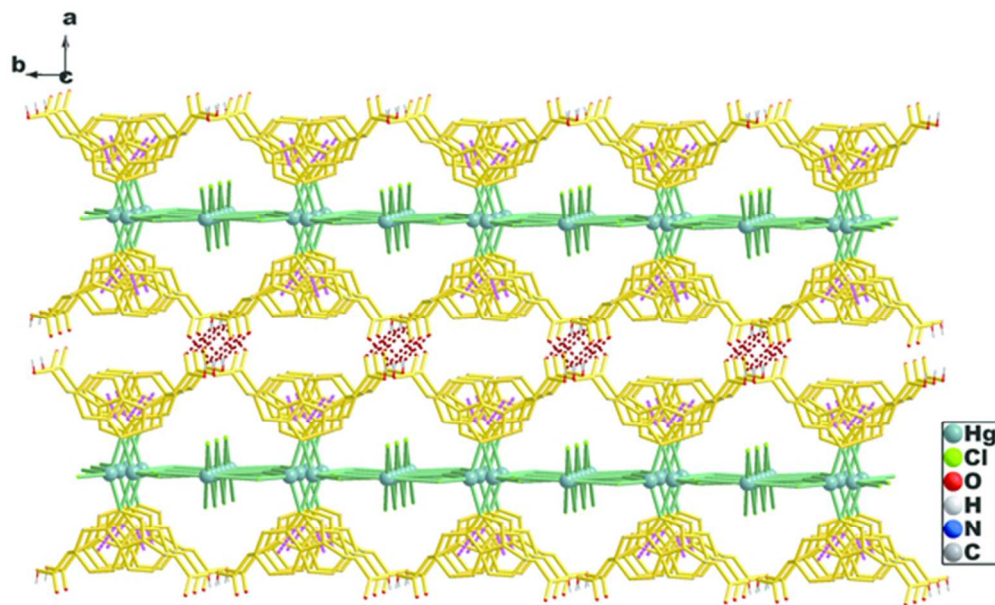
The coordination environments around Hg(II) ions in 6 (symmetry codes: A $1-x, y, 1/2-z$; B $1-x, 3-y, -z$).
70x59mm (300 x 300 DPI)



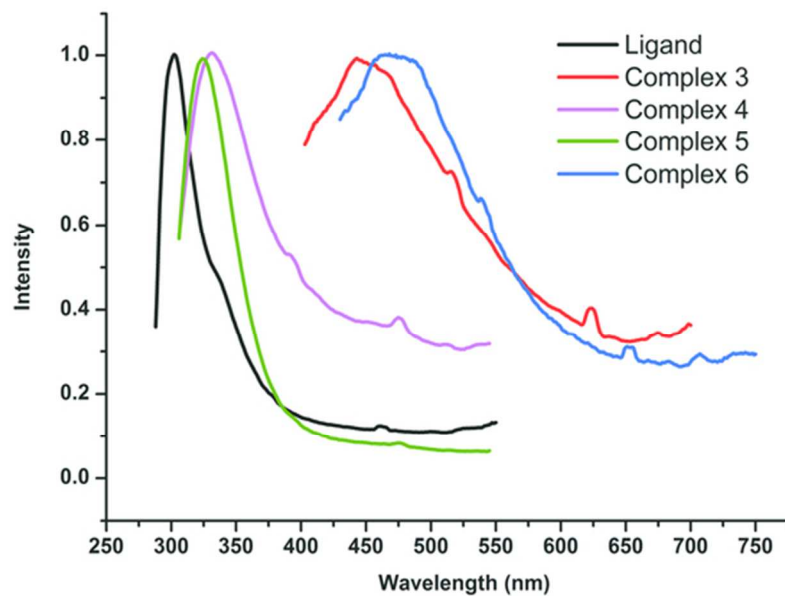
The 1D wavy coordination chain along the c axis sustained by Cl⁻ bridges. Hg, teal; C, grey; H, light grey; N, blue; O, red; Cl, bright green.
71x62mm (300 x 300 DPI)



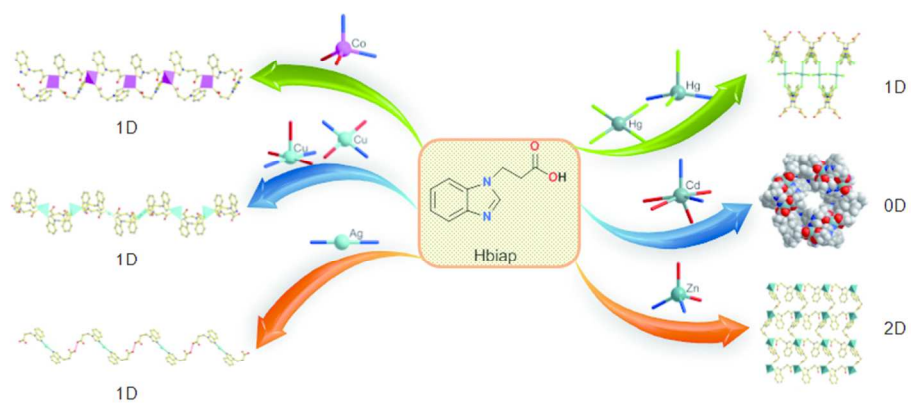
The 2D layered network along the bc plane formed by n...n stacking interactions.
51x32mm (300 x 300 DPI)



The 3D supramolecular framework sustained by n...n interactions and O-H...O hydrogen bonds. Hydrogen atoms not involved in hydrogen bonding are omitted for clarity.
51x32mm (300 x 300 DPI)



The normalized solid-state photoluminescent emission spectra of ligand Hbiap and complexes 3–6 at room temperature.
58x41mm (300 x 300 DPI)



80x39mm (300 x 300 DPI)